PHILOSOPHICAL TRANSACTIONS OF THE ROYAL SOCIETY A MATHEMATICAL, PHYSICAL & ENGINEERING SCIENCES

Melting Study of a Peridotite KLB-1 to 6.5 GPa, and the Origin of Basaltic Magmas

Eiichi Takahashi, Takeshi Shimazaki, Yasunori Tsuzaki and Hideto Yoshida

Phil. Trans. R. Soc. Lond. A 1993 **342**, 105-120
doi: 10.1098/rsta.1993.0008

Melting study of a peridotite KLB-1 to 6.5 GPa, and the origin of basaltic magmas

By Eiichi Takahashi[1], Takeshi Shimazaki[1], Yasunori Tsuzaki[1] and Hideto Yoshida[2]

[1] *Earth and Planetary Sciences, Tokyo Institute of Technology, 2-12-1 Ookayama, Meguro-ku, Tokyo 152, Japan*

[2] *Geological Institute, Faculty of Science, Tokyo University, 7-2-1 Hongo, Bunkyo-ku, Tokyo 113, Japan*

With a newly established multi-anvil press in the Tokyo Institute of Technology, we have carried out a series of melting experiments on peridotite KLB-1 up to 6.5 GPa. Melt fractions of the peridotite were determined in a wide P–T range using extensive X-ray mapping analysis of run products by EPMA and a digitalized back-scattered electron image technique. Compositions of partial melts and solid residues were determined in the whole melting range up to 6.5 GPa. Given quantitative information on mantle melting, we discuss conditions of melting of various basalt magmas and the nature of their source materials. Our conclusions are consistent with the hypothesis that typical mid oceanic ridge basalts represent low pressure (*ca.* 1 GPa), low temperature ($T_P \approx 1300$ °C) partial melting products of mantle peridotite. Island arc picritic tholeiites may also be regarded as partial melts of a peridotitic source, at 1–2 GPa pressures and T_P ranging from 1400 to 1500 °C. However, proposed primary magmas for Hawaiian tholeiite are difficult to produce by partial melting of typical mantle peridotite at any depth under anhydrous conditions. Source materials for magmas in large hotspots (e.g. Hawaii, Iceland and some continental flood basalts (CFBS)) may be anomalously enriched in FeO and TiO_2 relative to typical upper mantle peridotites such as KLB-1.

1. Introduction

Experimental melting studies on mantle materials have been attempted by many workers to understand the origin of magmas in the Earth. Progress in recent numerical calculations concerning the dynamics of mantle materials and the physics of magma generation (McKenzie 1984; McKenzie & Bickle 1988; Watson & McKenzie 1991) has demonstrated the usefulness and need for such experimental data. We have carried out a series of melting experiments on mantle peridotites (Takahashi & Kushiro 1983; Takahashi & Scarfe 1985; Takahashi 1986*a*; Ito & Takahashi 1987). However, the phase diagrams currently available prove to be still incomplete, if numerical calculations of mantle melting dynamics are to be carried out. For example, there is no reliable information on the temperature dependence of partial melting at $P \geqslant 3$ GPa. Moreover, low pressure experimental data on melt fractions already published (Mysen & Kushiro 1977; Jaques & Green 1980) show significant discrepancies. Lack of detailed information on melt compositions at pressures above 3 GPa, sets limitations on the discussions of the origin of high MgO magmas.

Phil. Trans. R. Soc. Lond. A (1993) **342**, 105–120
Printed in Great Britain

The main purpose of this study is to determine an accurate phase diagram for mantle peridotite KLB-1 over a wide range of pressures and temperatures. Special care was taken to determine precisely pressures and temperatures for experiments above 4 GPa. Because accuracy in experimental temperatures is critically important, we first determined pressure corrections on thermocouple e.m.f.s. Pressure and temperature were then calibrated by measuring melting curves of gold and lead by a differential thermal analysis (DTA) method. To determine melt fractions in high pressure run products ($P \geqslant 3$ GPa), where partial melts crystallized completely during quenching (Takahashi 1986*a*, fig. 10), extensive X-ray mapping analysis was carried out. The present paper summarizes the above works (details will be published separately): (1) pressure corrections on thermocouple e.m.f.s (Tsuzaki & Takahashi 1993); (2) quantitative determination of melt fractions using X-ray mapping analysis (Yoshida & Takahashi 1993); and (3) phase relations of peridotite KLB-1 up to 15 GPa (Shimazaki & Takahashi 1993).

2. Experimental procedures

Methods and procedures for experiments below 3 GPa are similar to those reported in previous studies (Takahashi & Kushiro 1983). To reduce iron loss from the specimen and minimize chemical contamination from the container, a ribbon of Re foil was used to support the specimen in 1 atm† experiments. A Re foil was also used as an inner capsule instead of graphite in piston-cylinder experiments at 0.8 and 1.5 GPa. Compared with graphite, the redox state of the experimental charges inside the Re–Pt double capsules may be more oxidizing.

A multi-anvil press (SPI-1000) was designed by Takahashi and constructed by the Riken Co. in 1991 and installed in the ultrahigh-pressure experimental petrology laboratory of the Tokyo Institute of Technology. The SPI-1000 consists of a main frame, 1000 t uniaxial hydraulic ram and of a guideblock system to drive the multi-anvils. The multi-anvils are double staged and with newly designed bucket-type guideblocks to drive the cubic–octahedral anvils. Like double-stage multi-anvil presses in other laboratories (Ito *et al.* 1984), pressure media of various octahedral sizes can be used in SPI-1000 by changing the final truncation size of the tungsten carbide anvils. In the present experiments, an MgO pressure medium of 18 mm edge length (18 M) octahedron was used for the experiments at 4.6 and 6.5 GPa. The 18 M octahedron was compressed with tungsten carbide anvils using an edge length truncation of 11 mm. This assembly is suitable up to 11 GPa (see figure 4 for pressure calibration). Higher pressures can be achieved by reducing the pressure medium and truncation.

Both the heating and the hydraulic system of the SPI-1000 are operated by programmable controllers. Rates of compression and decompression, as well as heating and cooling, can be digitally programmed up to a pattern with 20 segments. In most experiments, total decompression time was programmed to be more than several hours (figure 1). In high pressure experiments, the peridotite specimens were kept at 1500 °C for 20–30 min, before reaching the desired melting temperature. This was done to let the subsolidus mineral assemblage adjust to the experimental pressure. Fluctuations in oil pressure and furnace temperature were of the order of ± 1 t or ± 3 °C. An example of a run record is given in figure 1.

† 1 atm $\approx 10^5$ Pa.

PHILOSOPHICAL TRANSACTIONS OF THE ROYAL SOCIETY A MATHEMATICAL, PHYSICAL & ENGINEERING SCIENCES

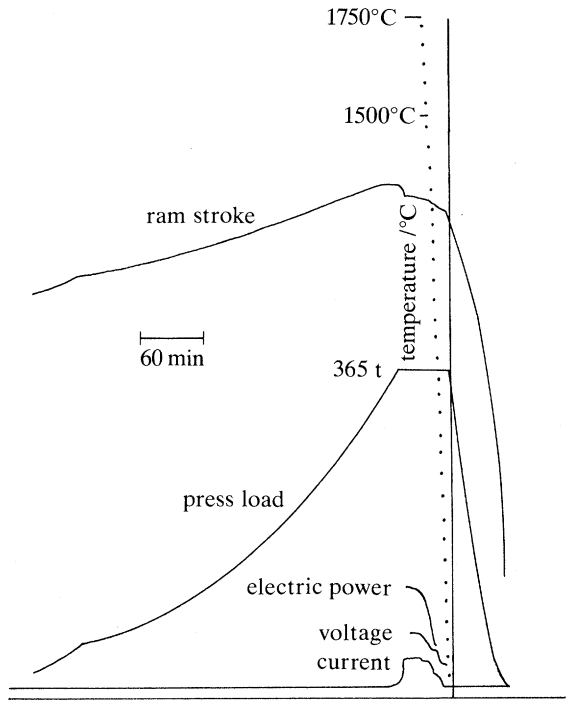

Figure 1. Run records for an experiment conducted at 6.5 GPa, 1750 °C and 20 min. In the SPI-1000 apparatus, both the hydraulic unit and the heating unit are controlled through a program and their fluctuations are very small (±1 t and ±3 °C).

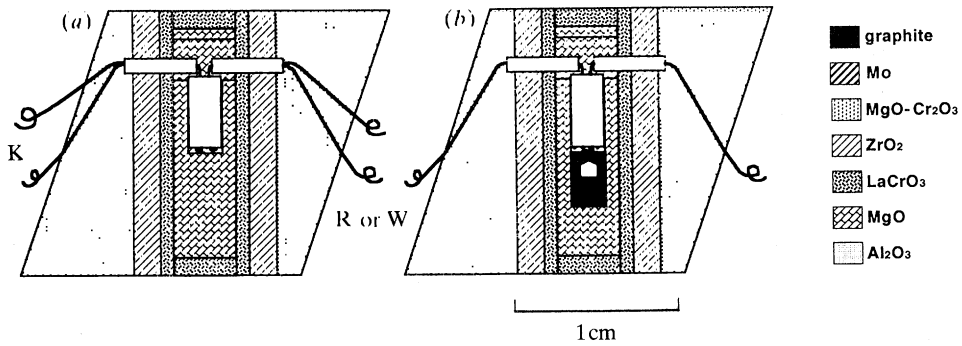

Figure 2. Furnace assemblies used for present experiments with the SPI-1000: (*a*) for thermocouple correction; (*b*) for melting experiment.

To avoid the temperature underestimation problems pointed out by Herzberg *et al.* (1990), the furnace assemblages shown in figure 2 were used in the present study (cf. Takahashi 1986*a*, fig. 2). To determine pressure effects on thermocouple e.m.f.s, the furnace assembly shown in figure 2*a* was used. Two sets of thermocouples were simultaneously used to record differences between their e.m.f.s at different pressures. K-, R- and W-type thermocouples (K, Chromel–Almel; R, Pt–Pt13% Rh; W, W5% Re–W26% Re) were tested. Apparent temperature differences between two thermocouple sets were recorded during heating and cooling cycles, at temperature intervals of 200 °C. The results obtained during the first heating cycles, at given

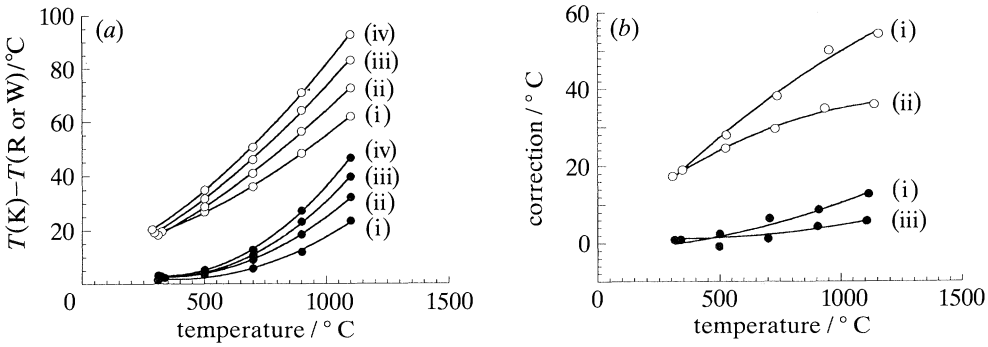

Figure 3. Experimental results for pressure corrections on thermocouple e.m.f.s. (*a*) Differences in apparent temperature readings with reference to the type-K thermocouple (Chromel–Almel). (i) 300 t; (ii) 400 t; (iii) 500 t; (iv) 600 t. (*b*) Absolute pressure corrections on e.m.f.s of the type-R (Pt–Pt 13 % Rh, —○—) and the type-W (W5 % Re–W26 % Re, —●—) thermocouples. (i) 11.5 GPa; (ii) 5.7 GPa; (iii) 7.7 GPa.

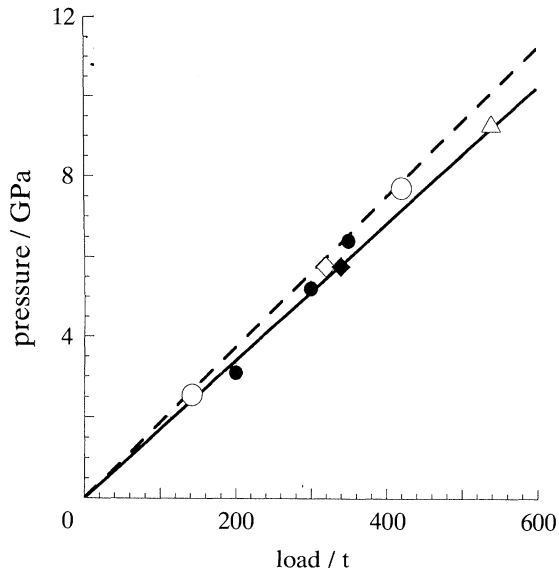

Figure 4. Pressure calibrations for the 18M type pressure cell in the SPI-1000 apparatus. Broken line is the room temperature calibration by Bi(I/II) and Bi(III/V) phase transitions. Solid line is the high temperature calibration determined with phase transitions of Fe_2SiO_4 (olivine/spinel) and SiO_2 (coesite/stishovite) at 1200 °C. Pressures determined by the melting curve of gold (●) by DTA (see figure 2*c*) coincide with the high temperature calibration line. ○, Bi; ◇, ◆, Fe_2SiO_4; △, SiO_2.

pressures, are plotted in figure 3*a*. Absolute pressure corrections for K-type thermocouple e.m.f.s., were calculated according to the method described by Getting & Kennedy (1970, and references therein). Absolute pressure corrections on R- and W-type thermocouple e.m.f.s (figure 3*b*) were calculated from the temperature differences (figure 3*a*) and the calculated absolute pressure corrections on K-type e.m.f.s. As e.m.f. pressure corrections for W-type thermocouples are very small, at least up to $P = 11.5$ GPa (figure 3*b*), in this study we used only W-type thermocouples.

Pressure calibrations were carried out with three independent methods (figure 4). Room temperature calibrations were established with phase transitions in Bi(I/II)

and Bi(III/V) by resistance change. High temperature (1200 °C) calibrations were made by observing phase changes in Fe_2SiO_4 (olivine/spinel) and SiO_2 (coesite/stishovite) by quenching technique. High temperature calibration points are 9% lower in pressure generation efficiency than room temperature calibration.

To further check the accuracy of pressure and temperature calibration, we conducted a series of DTAs to determine melting curves for Au and Pb. Mirwald *et al.* (1975) determined melting curves for Au and Pb up to 6 GPa by a piston-cylinder apparatus. The pressure was calculated from the observed DTA signals obtained at given press loads. Pressure calibration data for Au are plotted on figure 4 and are located on the high temperature calibration curve established by phase transitions in Fe_2SiO_4 and SiO_2 at 1200 °C. Because melting curves for metals have small dT/dP slopes, temperature measurements must be very accurate to read pressures from the melting curve. The fit in figure 4, therefore, demonstrates that both pressure and temperature calibrations and their reproducibility in our multi-anvil system, are very accurate. The validity of our pressure corrections on thermocouple e.m.f.s is also supported. Levels of uncertainties in pressures and temperatures in the present experiments would be ± 0.1 GPa and ± 5 °C, respectively, well within typical uncertainty ranges in conventional piston-cylinder experiments.

3. The peridotite KLB-1

Starting material used in the present experiments is a powdered spinel lherzolite xenolith (KLB-1) already described by Takahashi (1986*a*). Bulk chemical compositions of KLB-1 and well-documented mantle peridotite xenoliths (spinel lherzolite) are shown in figure 5. It is clear that KLB-1 represents a fertile example of typical mantle peridotites. Coherent variations in the major element chemistry of upper mantle peridotites (UMPs) have been recognized (Kuno & Aoki 1970; Maaløe & Aoki 1977) and interpreted as due to successive extraction of basalt magmas from the mantle. The least MgO-rich members of the UMPs (including KLB-1), therefore, may be closer to the primitive composition of the Earth's mantle (Ringwood 1975; Jagoutz *et al.* 1979; Hart & Zindler 1987).

Pyrolite compositions used in experimental melting studies (see following references) are also shown in figure 5. By definition, pyrolite compositions depend largely on the selected basalts for the mixing calculations (Ringwood 1975). A pyrolite composition based on Hawaiian tholeiite (Jaques & Green 1980) is very enriched in TiO_2. On the contrary, a MORB-pyrolite composition frequently used in recent experiments (Falloon & Green 1988; Falloon *et al.* 1988) is enriched in FeO compared with UMPs (figure 5).

In our study, partial melts from KLB-1 were obtained for a wide pressure and temperature range. Because KLB-1 is a fertile peridotite, whose bulk chemical composition falls in the well-defined compositional cluster of UMPs (figure 5), our experimental results may be applicable to the discussion of the petrogenesis of basaltic magmas under various tectonic settings, provided that they derive from typical UMPs and that their melting conditions are nearly anhydrous. In other words, the present experimental results may be useful to discuss diversities in source rock compositions of basaltic magmas.

PHILOSOPHICAL TRANSACTIONS OF THE ROYAL SOCIETY A MATHEMATICAL, PHYSICAL & ENGINEERING SCIENCES

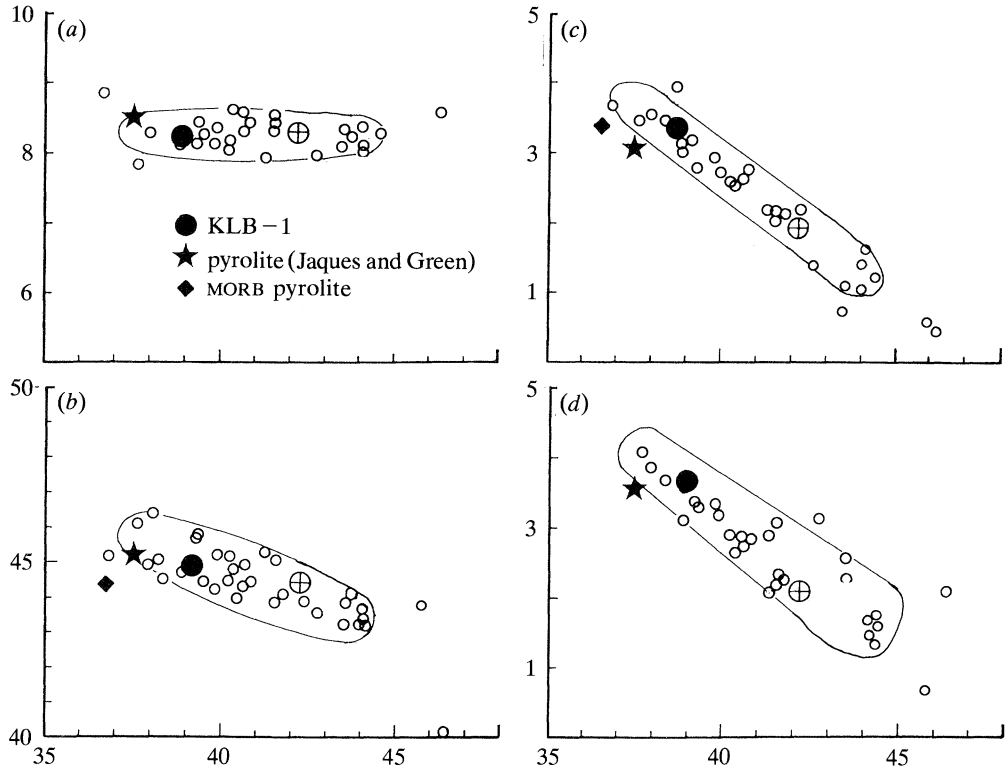

Figure 5. Bulk chemical compositions (in oxide wt %) of upper mantle peridotites (UMPS). See fig. 4 of Takahashi (1990) for data sources. Large circles with cross represent average composition of 384 spinel peridotite xenoliths by Maaløe & Aoki (1977). Composition of the starting material KLB-1 plots on the Fe-rich side of the well-defined compositional cluster of UMPS. In other words our experiments were conducted on a representative fertile composition of the Earth's upper mantle. Some pyrolite compositions experimentally tested are shown for comparison. (*a*) FeO; (*b*) SiO_2; (*c*) CaO; (*d*) Al_2O_3. Horizontal axes, MgO.

4. Melt fraction as a function of P and T

The degree of melting of mantle peridotite (ϕ) at given pressure and temperature ϕ (P, T) is one of the most important parameters to constrain the isentropic melting paths of uprising mantle materials (McKenzie 1984). At present, ϕ is determined only by experiments. Most experimental data on the melt fraction, however, are limited to low pressures, not greater than 1.5 GPa. Because of the lack of experimental data, McKenzie & Bickle (1988) assumed homologous relations on the $\phi(T)$ curve with pressure (see their fig. 6), i.e. they assumed that the degree of partial melting of a given peridotite does not change with pressure when temperature is normalized by the temperature intervals between the solidus and liquidus. This assumption is insufficient, because solidus melts change towards olivine rich compositions with increasing pressure (Takahashi & Kushiro 1983), i.e. the melting behaviour of mantle peridotite should become more eutectic with increasing pressure (Mysen & Kushiro 1977).

Melt fractions have been estimated by SEM (Jaques & Green 1980) and by β-track mapping analysis (Mysen & Kushiro 1977) of experimental run products. Mass

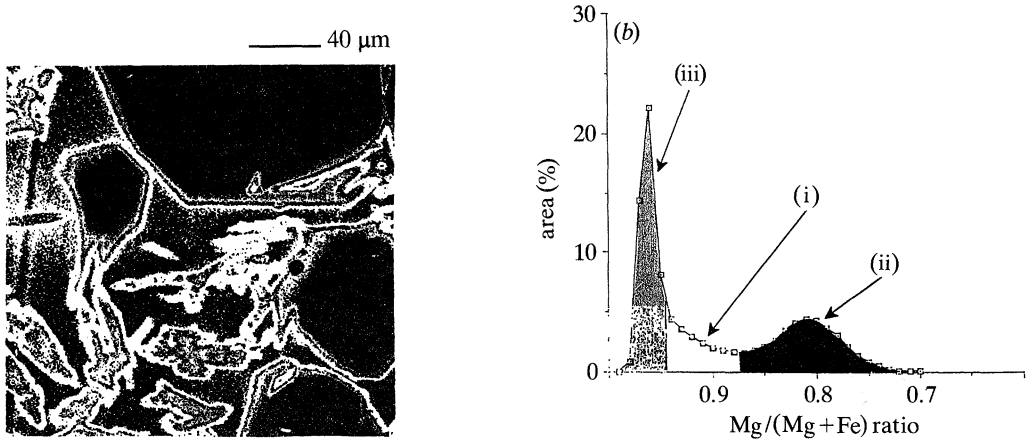

Figure 6. Example of X-ray mapping analysis on experimental run product (1.5 GPa, 1650 °C, 10.5 h). (*a*) Concentration map of Mg, consisting of large euhedral olivines (50–200 μm), small pyroxene quench crystals (10–50 μm) and glass. Olivines are mantled by thin rinds of overgrowth. Original photo was in 24 pseudo colours corresponding to MgO concentration. Approximately 30% of the original area (400×400 μm^{-2}) is shown. (*b*) The Mg/(Mg+Fe) ratios of the 160000 point analyses were computed by using a calibration line method. Quench crystals (i), overgrowth and glass (ii) can be distinguished from the stable olivine crystals (iii) by using the Mg/(Mg+Fe) ratios.

balance calculations may be useful especially at higher temperatures, where peridotites consist only of olivine and partial melt. Peridotite partial melts are unquenchable at pressures above about 2 GPa. Even at low pressures (when glass is formed in the run products) melt compositions are significantly modified due to overgrowth of adjacent solid phases (Jaques & Green 1979; Takahashi & Kushiro 1983; see also figure 6*a*).

To obtain reliable $\phi(P, T)$ data for KLB-1, we carried out an extensive digital X-ray mapping analysis of our run products, with a fully automated electron microprobe analyser JCMA-733MkII, at the University of Tokyo. Five spectrometers were used in fixed positions, to collect characteristic X-rays for Mg, Fe, Ca, Al and Cr. The X-ray countings were made for 40 ms for each point analysis and repeated at 1 μm grid intervals within a 400×400 μm^2 area, on the polished surface of our run products. To check spatial heterogeneities, the digital mapping was repeated at least at two locations within a single run product. With the aid of high speed stepwise motors for stage motion, the total counting time for the each 400×400 μm^2 area, was reduced to 3 h. To readily convert intensities into concentrations, we used a calibration line method for the above elements. Calibration lines were determined at the beginning of each analysis by carefully measuring 20 known standards mostly made out of peridotite constituent minerals. The resolution of our digital mapping analysis is good enough to identify very small changes in mineral composition (i.e. less than 0.3 mol% forsterite in olivine). The digital X-ray map is very useful in identifying stable mineral phases, overgrowth and quench crystals, glass and relics. An example of the MgO X-ray map of a run product obtained at 1.5 GPa and 1650 °C is shown in figure 6*a*. Modal proportions of olivine, quench crystals and glass, calculated from the Mg/(Mg+Fe) ratio for the same charge, are shown in figure 6*b*.

For experimental charges with uneven melt distributions, digital back-scattered electron image (BEI) analyses were carried out. In digital BEI, relative darkness of matter was converted into 16 pseudo colours, thereby used to distinguish quench

Table 1. *Run conditions, melt fractions and melt compositions*

P	T/°C	t/min	melt (%)	SiO_2	MgO	FeO	CaO	Al_2O_3	Na_2O	TiO_2
1 atm	1175	3330	5	—	—	—	—	—	—	—
1 atm	1204	2580	16	55.0	8.5	5.7	12.5	15.3	2.2	0.7
1 atm	1247	450	22	—	—	—	—	—	—	—
1 atm	1300	2100	31	54.9	15.0	7.8	8.8	12.0	0.6	0.4
1 atm	1350	360	37	—	—	—	—	—	—	—
1 atm	1400	360	45	51.2	22.5	9.1	6.5	9.5	0.4	0.3
1 atm	1500	60	49	49.6	24.4	10.3	6.5	7.9	0.2	0.3
1 atm	1600	420	64	47.8	29.5	9.4	5.4	6.5	0.1	0.2
0.8 GPa	1300	960	—	51.3	10.1	5.3	12.5	17.7	1.5	0.6
0.8 GPa	1350	240	—	50.9	11.3	6.5	11.6	17.0	1.4	0.6
0.8 GPa	1400	480	—	51.7	15.5	7.2	10.1	13.3	1.2	0.4
0.8 GPa	1450	60	—	49.8	16.6	7.4	9.8	14.1	1.2	0.4
0.8 GPa	1500	120	—	50.7	25.0	8.0	6.1	8.7	0.5	0.3
1.5 GPa	1400	140	17	—	—	—	—	—	—	—
1.5 GPa	1450	210	24	48.8	15.0	7.6	11.3	14.7	1.5	0.5
1.5 GPa	1500	40	43	—	—	—	—	—	—	—
1.5 GPa	1550	180	—	50.1	20.4	7.8	7.9	11.5	1.2	0.4
1.5 GPa	1600	150	50	—	—	—	—	—	—	—
1.5 GPa	1650	630	52	—	—	—	—	—	—	—
1.5 GPa	1700	36	56	—	—	—	—	—	—	—
3.0 GPa	1550	1020	—	47.0	19.2	7.8	12.2	11.0	1.2	0.9
4.6 GPa	1700	20	15	—	—	—	—	—	—	—
4.6 GPa	1750	20	22	47.6	19.8	11.3	7.8	10.2	1.1	0.6
4.6 GPa	1800	20	55	48.0	26.9	9.5	5.5	8.3	0.5	0.4
4.6 GPa	1850	10	65	47.2	34.3	8.4	3.7	5.2	0.3	0.2
4.6 GPa	1900	5	78	47.0	33.8	8.1	3.9	5.4	0.3	0.1
6.5 GPa	1850	20	23	—	—	—	—	—	—	—
6.5 GPa	1900	15	34	49.3	23.4	10.0	7.8	7.1	0.8	0.4
6.5 GPa	1950	15	72	49.0	29.4	8.7	4.9	6.8	0.1	0.2
6.5 GPa	2000	10	75	48.1	32.4	8.6	4.0	5.7	0.4	0.1

crystals from stable solid phases. Compared with the digital X-ray mapping, the resolution is poor (0.5 mol % in olivine solid solution) but a large area covering the entire run product (1×1 mm^2) can be analysed in minutes.

Because the X-ray mapping and the digital BEI were taken on polished surfaces of run products, these analyses could be in error if melts and solids are unevenly distributed. This effect may become severe in experimental run products with a high degree of partial melting. We therefore conducted mass balance calculations using chemical analyses of melt and olivine and the bulk composition of KLB-1. The $\phi(P, T)$ curves for the peridotite KLB-1 were estimated from experimental results at 1 atm, 1.5 GPa, 4.6 GPa and 6.5 GPa (see table 1 and figure 7*b*). In the $\phi(T)$ curves obtained at 1 atm and 1.5 GPa, melt fraction changes significantly near both the solidus and the liquidus. Accordingly, there is a large temperature interval between $\phi = 0.4$ and 0.6 at low pressures. This melting behaviour is consistent with previous observations (McKenzie & Bickle 1988, fig. 6). The two-stage melting may be attributed to eutectic melting of pyroxenes and olivine near the solidus and disappearance of magnesian olivine near the liquidus. At pressures above about 3 GPa, however, this two-stage melting mode becomes less prominent (figure 7*b*).

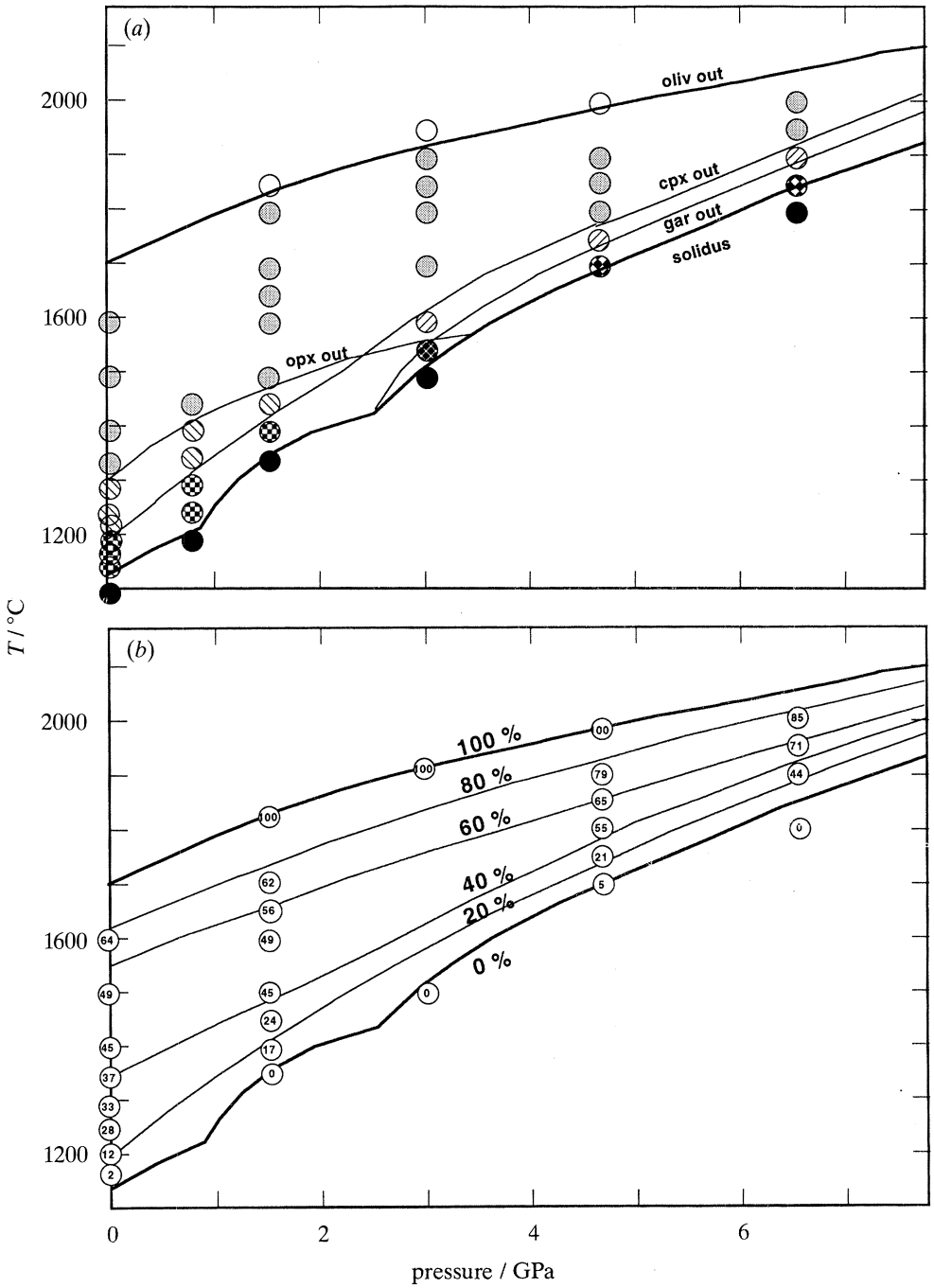

Figure 7. (*a*) Melting phase relations of peridotite KLB-1. All experimental data points at 1 atm, 0.8 GPa, 4.6 GPa and 6.5 GPa were newly obtained. Part of the data at 1.5 and 3 GPa were taken from Takahashi (1986*a*). (*b*) Melt fractions of peridotite KLB-1 determined by X-ray mapping analysis (see figure 6), digitalized BEI techniques, and mass balance calculations. Eutectic behaviour become more prominent with increasing pressure (cf. figure 7*b* with figure 7*a* of McKenzie & Bickle (1988)).

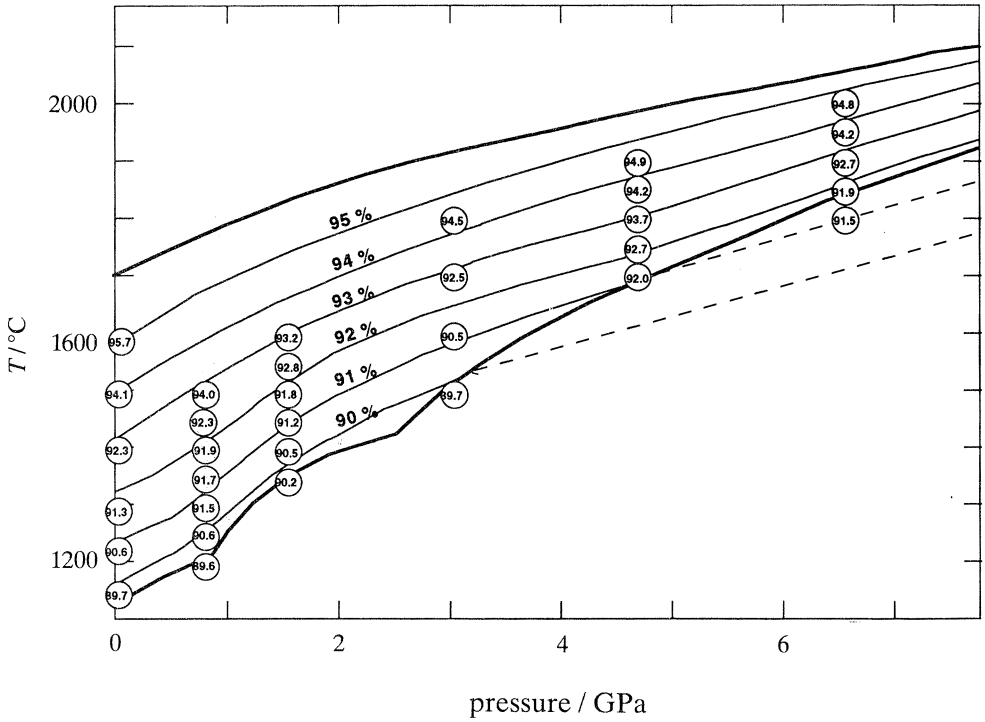

Figure 8. Average forsterite content of olivine residues.

5. Melt compositions as a function of P and T

Melting phase relations of the anhydrous peridotite KLB-1 are summarized in figure 7*a*. Some experimental results at 1.5 GPa and 3.0 GPa taken from Takahashi (1986*a*) are also reported. Run conditions and information on melt fractions and melt chemistry are summarized in table 1. Compositions of residual olivines are summarized in figure 7*b*. Because of the presence of Fe-rich garnet in subsolidus conditions at $P \geqslant 3$ GPa, the Mg/(Mg+Fe) ratio of subsolidus olivine becomes higher than in the starting material (figure 8).

Partial melt compositions were determined by directly analysing quenched partial melts (either glass or quench crystals). For experiments at $P = 1$ atm, glass compositions obtained by EPMA (from large glass pods not less than 20 μm diameter) were cross-checked by using olivine–liquid Fe–Mg partitioning data ($K_D(\mathrm{Fe/Mg})^{\alpha\text{–liq}} =$ 0.30 to 0.37 (Takahashi 1978)). Because of increasing overgrowth effects, glass compositions in the peridotite matrix obtained at 0.8 and 1.5 GPa are less reliable. Melt compositions obtained in large melt pods and satisfying the above K_D constraints are shown in table 2. To determine reliable melt compositions at 0.8 and 1.5 GPa, a series of experiments using the basalt/peridotite sandwich technique (Takahashi & Kushiro 1983) have been conducted. Additional basalt components (table 2) were carefully chosen not to alter the composition of peridotite matrix melts. A minimum quantity of basalt powder was added to the peridotite KLB-1 to obtain melt compositions similar to those of pure KLB-1. Compositions of melts resulting from the basalt/peridotite sandwich experiments, are compared with partial melt compositions of pure KLB-1 when direct EPMA analysis of matrix glass

Table 2. *Chemical compositions of peridotite partial melts*

(Compositions determined by direct EPMA analysis of quenched glass and those determined with the basalt/peridotite sandwich technique of Takahashi & Kushiro (1983).)

	0.8 GPa, 1325 °C, 18 h		0.8 GPa, 1500 °C, 2 h		starting basalts	
	KLB-1	KLB-1/FU12	KLB-1	KLB-1/T-16	FU12	T-16
SiO_2	51.4	51.2	50.4	48.7	46.8	46.5
TiO_2	0.5	0.5	0.3	0.3	0.6	0.5
Al_2O_3	15.0	14.6	8.6	8.1	15.0	14.2
FeO	6.9	7.0	7.9	8.3	9.1	7.4
MgO	12.6	13.5	24.9	26.7	13.1	15.9
CaO	11.9	11.3	6.1	6.2	14.0	13.3
Na_2O	1.2	1.3	0.5	0.5	1.5	1.6
K_2O	0.04	0.05	0.00	0.10	0.02	0.02
composition of olivine residues and Fe–Mg partition coefficients						
Fo	91.5	91.2	94.2	93.9		
Kd(Fe/Mg)	0.30	0.33	0.34	0.37		

was successful (table 2). Agreements between melt compositions obtained by the two methods are very good in both major and minor elements (table 2).

In experimental run products obtained by the multi-anvil apparatus, partial melts were segregated within 10–20 min of run durations. This may be due to large melt fractions in most of run products (figure 7*b*). Larger temperature gradients (typically less than 50 °C mm^{-1}) in the multi-anvil cell (figure 2) compared with those in piston-cylinder cells (not more than 10 °C mm^{-1}) may be another factor in enhancing the melt segregation. The segregated melt compositions have been determined by broad-beam EPMA analysis.

Observed melt compositions are summarized in table 1 and some are plotted in figure 9. Because we have determined melt fractions $\phi(P, T)$ in figure 8*b*, and olivine is the only residual phase in the high temperature regions ($\phi \geqslant 0.4$, cf. figure 7*a* with *b*), melt compositions can be calculated by mass balance. Agreements between the calculated and measured results were acceptable except for Al_2O_3 and Na_2O. Disagreements may be due (at least in part) to uncertainty in the EDS X-ray analysis we used to determine the melt compositions. In fact, in EDS analysis, deconvolution of very small X-ray peaks for Al and Na from the dominant Mg peak may be difficult. Loss of Na during the EDS analysis was avoided by using relatively large beam sizes. In 1 atm runs, however, loss of Na during the experiments was significant and melt compositions are not reliable for sodium at $T \geqslant 1300$ °C.

6. Primary magma compositions and their origin

Given the $\phi(P, T)$ curves (figure 7*b*) and the melt compositions (figure 9) for typical upper mantle peridotite KLB-1, primary magma compositions and the magma production rate can be calculated for isentropic decompressional melting paths with various potential mantle temperatures (McKenzie 1984; McKenzie & Bickle 1988). If pressure effects on the $\phi(T)$ curves are taken into account, calculation schemes may become rather complicated. Before such numerical calculations are made, we discuss three representative melting régimes with reference to proposed primary magmas. In decompressional melting of mantle upwelling flow with $T_p = 1280$, 1550 and 1800 °C,

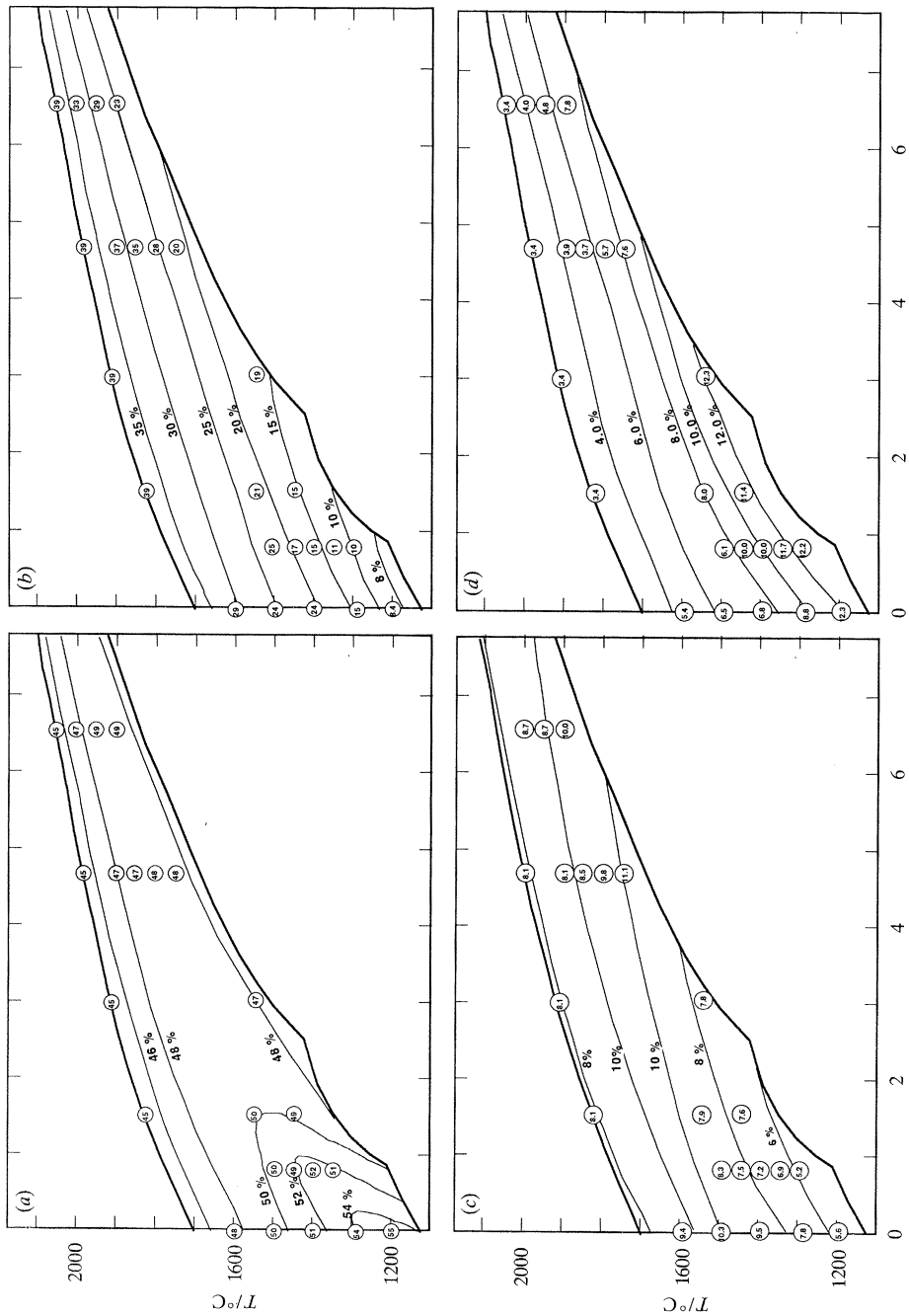

Figure 9. Partial melt compositions of peridotite KLB-1 up to 6.5 GPa. Isoplethal lines were fitted by eye. (*a*) SiO_2; (*b*) MgO; (*c*) FeO; (*d*) CaO.

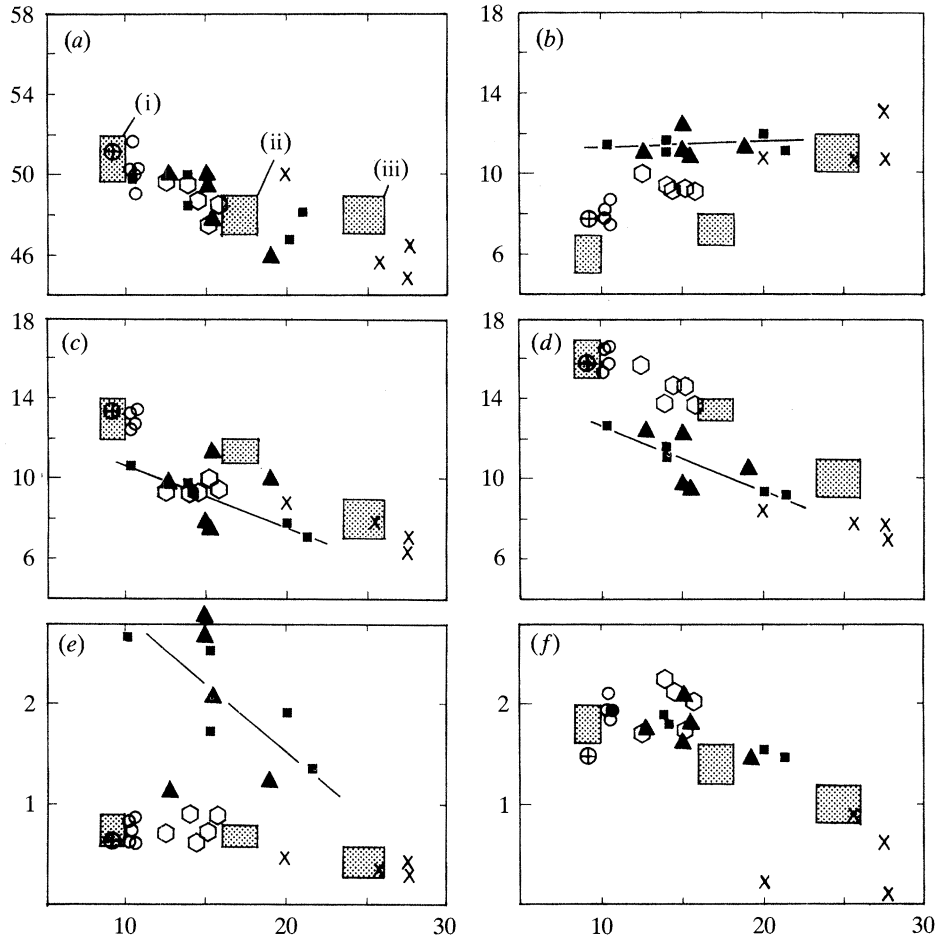

Figure 10. Expected initial melt compositions for decompressional melting of upper mantle peridotite for PMTs of (i) 1280, (ii) 1550 and (iii) 1800 °C are shown as shaded areas. Compositions of proposed primary magmas for MORBs (open circles), island arc tholeiites (open hexagons), Hawaiian tholeiites (solid squares), some continental flood basalts (solid triangles) and Archean komatiites (crosses) are shown. These rock compositions were taken from BVSP (1981), Takahashi (1986*b*) and Tatsumi *et al.* (1983). Large open circles with cross represent the average of 218 primitive MORB glass analyses by Melson *et al.* (1977). In oxide weight %, (*a*) SiO_2; (*b*) FeO; (*c*) CaO; (*d*) Al_2O_3; (*e*) TiO_2; (*f*) Na_2O. Horizontal axes, MgO.

partial melting of UMPs will take place at $\leqslant 1$ GPa, $\geqslant 4$ GPa, and $\geqslant 7$ GPa. Partial melting in the above régimes corresponds to the genesis of MORBs (McKenzie & Bickle 1988), Hawaiian tholeiite (Watson & McKenzie 1991) and Archean komatiites (Bickle *et al.* 1977; Takahashi 1990).

Expected initial melt compositions within the first $\geqslant 20$ % of batch partial melting under the above *P*–*T* conditions were estimated based on our new experimental results in table 1 and in figure 9. The estimated initial melt compositions are shown in figure 10. As proposed by McKenzie & Bickle (1988), primary MORB magma compositions plot very close to the expected melt compositions for $T_P = 1280$ °C. According to our experiments, the MgO content of the near solidus melt in this region is between 8 and 9 wt % (figure 9*b*), whereas estimated MORB primary magmas are slightly higher in MgO (10–11 wt %, see figure 10). On the other hand, the average

of 218 primitive MORB glass analyses (open circle with cross in figure 10) by Melson *et al.* (1977) is identical to our expected composition except for minor differences in FeO and Na_2O. The deficiency in Na_2O in Melson *et al.*'s glass analyses may be due to Na volatilization during EPMA analyses. The higher FeO content in natural rocks with respect to experimental results may be explained by assuming that *ca.* 10% of iron in the MORB magmas is represented by ferric-iron but experiments were conducted under virtually ferric-iron free conditions due to the redox conditions imposed by the Re–Pt double capsule.

The genesis of MORB magmas is a fundamental problem in Earth sciences and, therefore, has been investigated by a great number of workers (e.g. Falloon & Green 1988; Kinzler & Grove 1992). We emphasize that the present study adds experimental support for the theory of MORB magma generation in relatively low pressure and temperature régimes (Green & Ringwood 1967; Presnall *et al.* 1979; Takahashi & Kushiro 1983; Fujii & Boughalt 1983; Presnall & Hoover 1984; Fujii & Scarfe 1985; Klein & Langmuir 1987; McKenzie & Bickle 1988).

Some primitive island-arc tholeiites are plotted in figure 10 (open hexagons). They plot in the compositional range of partial melts expected for T_P between 1280 and 1550 °C. Except for minor deficiencies in CaO and slight enrichment in Na_2O, their chemical signatures are very similar to those of MORB primary magmas (open circles). Estimated pressure and temperature conditions (1–2 GPa and *ca.* 1400 °C) for the primary island-arc tholeiite by Tatsumi *et al.* (1973) are consistent with our peridotite melting study. It follows that source materials for island-arc tholeiites may be peridotites similar to KLB-1.

Estimated primary basalt magma compositions for Hawaiian shield volcanoes differ among authors with different assumptions and different methods of calculation. Because primitive Hawaiian tholeiites are olivine saturated, proposed primary magmas for Kilauea and Mauna Loa (Irvine 1979; BVSP 1980; Wright 1984; Wilkinson 1985) lie essentially on an olivine fractionation line (figure 10*b–e*). Notable features for the Hawaiian tholeiites compared with MORBs are their higher FeO and TiO_2 contents. Even taking the highest possible MgO content for the Hawaiian primary magma (MgO $\approx$ 20 wt%), their TiO_2 contents are still two to three times higher than the expected composition of peridotite partial melts (figure 10*e*). Their FeO content might be compatible with our estimation if the highest MgO is assumed. However, their FeO is significantly higher than expected KLB-1 partial melts if the MgO of primary Hawaiian tholeiite is lower than 15 wt% (figure 10*b*). Furthermore, both CaO and Al_2O_3 for Hawaiian primary magmas are considerably lower than our estimated partial melts for all MgO concentrations (figure 10*c*, *d*). Accordingly, we propose that source materials for Hawaiian tholeiite magmas are significantly different from the normal UMP predominant in mantle xenoliths and tectonic blocks (figure 5). The anomalous nature of source rock compositions for Hawaiian tholeiite have been discussed by several authors (e.g. Wright 1984; Wilkinson 1985, 1991). Based on a quantitative olivine fractionation model (Takahashi 1986*b*), we have estimated that source materials for the Hawaiian mantle plume may be more than 50% enriched in iron compared with common UMPs (Takahashi & Uto 1993).

It is very important to note that proposed primary magmas for continental flood basalt terrains show chemical characteristics very similar to those of the Hawaiian hotspot (figure 10). This may indicate that mantle plume components of deep origin underneath very large hotspots may be different from shallower mantle peridotites (UMPs) in major element chemistry.

Stimulating and helpful discussions by Professor D. McKenzie were the motivation of this study. Critical readings of the manuscript by Professor D. McKenzie, Dr K. G. Cox and Dr G. Caprarelli at various stages of its preparation are greatly acknowledged. This is a contribution of the Department of Earth and Planetary Sciences, Tokyo Institute of Technology, no. 6. We acknowledge grants 02402019, 04216203 and 04201121 from the Ministry of Education, Science and Culture, Japan.

References

Bickle, M. J., Ford, C. E. & Nisbet, E. G. 1977 The petrogenesis of peridotitic komatiites: evidence from high pressure melting experiments. *Earth planet. Sci. Lett.* **37**, 97–106.

BVSP 1981 *Basaltic volcanism on the terrestrial planets.* (1286 pages.) New York: Pergamon.

Falloon, T. J. & Green, D. H. 1988 Anhydrous partial melting of peridotite from 8 to 35 kb and petrogenesis of MORB. *J. Petrol.*: *Oceanic and Continental Lithosphere* (ed. M. A. Menzies & K. G. Cox), pp. 379–414.

Falloon, T. J., Green, D. H., Hatton, C. J. & Harris, K. L. 1988 Anhydrous partial melting of a fertile and depleted peridotite from 2 to 30 kb and application to basalt petrogenesis. *J. Petrol.* **29**, 1257–1282.

Fujii, T. & Bougault, H. 1983 Melting relations of a magnesian abyssal tholeiite and the origin of MORBs. *Earth planet. Sci. Lett.* **62**, 283–295.

Fujii, T. & Scarfe, C. M. 1985 Composition of liquids coexisting with spinel lherzolite at 10 kb and the genesis of MORBs. *Earth planet. Sci. Lett.* **20**, 18–28.

Getting, I. C. & Kennedy, G. C. 1970 Effect of pressure on the emf of chromel-alumel and platinum–platinum 10% rhodium thermocouples. *J. appl. Phys.* **41**, 4552–4562.

Green, D. H. & Ringwood, A. E. 1967 The genesis of basaltic magmas. *Contrib. Mineral. Petrol.* **15**, 103–190.

Hart, S. R. & Zindler, A. 1986 In search of a bulk-earth composition. *Chemical Geol.* **57**, 247–267.

Herzberg, C. T., Gasparik, T. & Sawamoto, H. 1990 Origin of mantle peridotite: constraints from melting experiments to 16.5 GPa. *J. geophys. Res.* **95**, 15779–15803.

Irvine, T. N. 1979 Rocks whose composition is determined by crystal accumulation and sorting. In *The evolution of the igneous rocks* (ed. H. S. Yoder Jr), pp. 245–306. Princeton University Press.

Ito, E. & Takahashi, E. 1987 Melting of peridotite at uppermost lower mantle conditions. *Nature, Lond.* **328**, 514–517.

Ito, E., Takahashi, E. & Matsui, Y. 1984 The mineralogy and chemistry of the lower mantle: an implication of the ultrahigh-pressure phase relations in the system MgO–FeO–SiO_2. *Earth planet. Sci. Lett.* **67**, 238–248.

Jagoutz, E., Palme, H., Baddenhausen, H., Blum, K., Cendales, M., Dreibus, G., Spettel, B., Lorenz, V. & Wänke, H. 1979 The abundance of major, minor and trace elements in the earth's mantle as derived from primitive ultramafic nodules. *Proc. Lunar. Planet. Sci. Conf.* **10**, 2031–2050.

Jaques, A. L. & Green, D. H. 1979 Determination of liquid compositions in experimental, high pressure melting of peridotite. *Am. Mineral.* **64**, 1312–1321.

Jaques, A. L. & Green, D. H. 1980 Anhydrous melting of peridotite at 0–15 kb pressure and the genesis of tholeiitic basalts. *Contrib. Mineral. Petrol.* **73**, 287–310.

Kinzler, R. J. & Grove, T. L. 1992 Primary magmas of mid-ocean ridge basalts. Parts I, II. *J. geophys. Res.* **97**, 6885–6906; 6907–6926.

Klein, E. M. & Langmuir, C. H. 1987 Global correlation of ocean ridge basalt chemistry with axial depth and crustal thickness. *J. geophys. Res.* **92**, 8089–8115.

Kuno, H. & Aoki, K. 1970 Chemistry of ultramafic nodules and their bearing on the origin of basaltic magmas. *Phys. Earth planet. Inter.* **3**, 273–301.

Maaløe, S. & Aoki, K. 1977 The major element composition of the upper mantle estimated from the composition of lherzolites. *Contrib. Mineral. Petrol.* **63**, 161–173.

McKenzie, D. 1984 The generation and compaction of partially molten rock. *J. Petrol.* **25**, 713–765.

McKenzie, D. & Bickle, M. J. 1988 The volume and composition of melt generated by extension of the lithosphere. *J. Petrol.* **29**, 625–679.

Melson, W. G., Byerly, G. R., Nelson, J. A., O'Hearn, T., Wright, T. L. & Vallier, T. 1977 A catalogue of major element chemistry of abyssal volcanic glasses. *Smithson. Contrib. Earth Sci.* **19**, 31–61.

Mirwald, P. W., Getting, I. C. & Kennedy, G. C. 1975 Low-friction cell for piston-cylinder high-pressure apparatus. *J. geophys. Res.* **80**, 1519–1525.

Mysen, B. O. & Kushiro, I. 1977 Compositional variations of coexisting phases with degree of melting of peridotite in the upper mantle. *Am. Mineral.* **62**, 843–865.

Presnall, D. C., Dixon, J. R., O'Donnell, T. H. & Dixon, S. A. 1979 Generation of mid-ocean ridge tholeiite. *J. Petrol.* **20**, 3–35.

Presnall, D. C. & Hoover, J. P. 1984 Composition and depth of origin of primary mid-ocean ridge basalts. *Contrib. Mineral. Petrol.* **87**, 170–178.

Ringwood, A. E. 1975 *Composition and petrology of the Earth's mantle.* (618 pages.) New York: McGraw-Hill.

Takahashi, E. 1978 Partitioning of Ni^{2+}, Co^{2+}, Fe^{2+}, Mn^{2+}, and Mg^{2+} between olivine and silicate melts: compositional dependence of partition coefficient. *Geochim. cosmochim. Acta* **42**, 1829–1844.

Takahashi, E. 1986*a* Melting of a dry peridotite KLB-1 up to 14 GPa: implications on the origin of peridotitic upper mantle. *J. geophys. Res.* **91**, 9367–9382.

Takahashi, E. 1986*b* Origin of basaltic magmas: implications from peridotite melting experiments and an olivine fractionation model. *Bull. Volcanol. Soc. Japan* (30th Anniversary Issue), S17–S40. (In Japanese with English abstract.)

Takahashi, E. 1990 Speculations on the Archean mantle: missing link between komatiite- and depleted garnet peridotite. *J. geophys. Res.* **95**, 15941–15954.

Takahashi, E. & Kushiro, I. 1983 Melting of a dry peridotite at high pressures and basalt magma genesis. *Am. Mineral.* **68**, 859–879.

Takahashi, E. & Scarfe, C. M. 1985 Melting of peridotite to 14 GPa and the genesis of komatiite. *Nature, Lond.* **315**, 566–568.

Tatsumi, Y., Sakuyama, M., Fukuyama, H. & Kushiro, I. 1983 Generation of arc basalt magmas and thermal structure of the mantle wedge in subduction zones. *J. geophys. Res.* **88**, 5815–5825.

Watson, S. & McKenzie, D. 1991 Melt generation by plumes: a study of Hawaiian volcanism. *J. Petrol.* **32**, 501–537.

Wilkinson, J. F. G. 1985 Undepleted mantle composition beneath Hawaii. *Earth planet. Sci. Lett.* **75**, 129–138.

Wilkinson, J. F. G. 1991 Mauna Loan and Kilauean tholeiites with low ferromagnesian-fractionated 100 $Mg/(Mg+Fe^{2+})$ ratios: primary liquids from the upper mantle? *J. Petrol.* **32**, 863–907.

Wright, T. L. 1984 Origin of Hawaiian tholeiite: a metasomatic model. *J. geophys. Res.* **89**, 3233–3252.

PHILOSOPHICAL TRANSACTIONS OF THE ROYAL SOCIETY A MATHEMATICAL, PHYSICAL & ENGINEERING SCIENCES

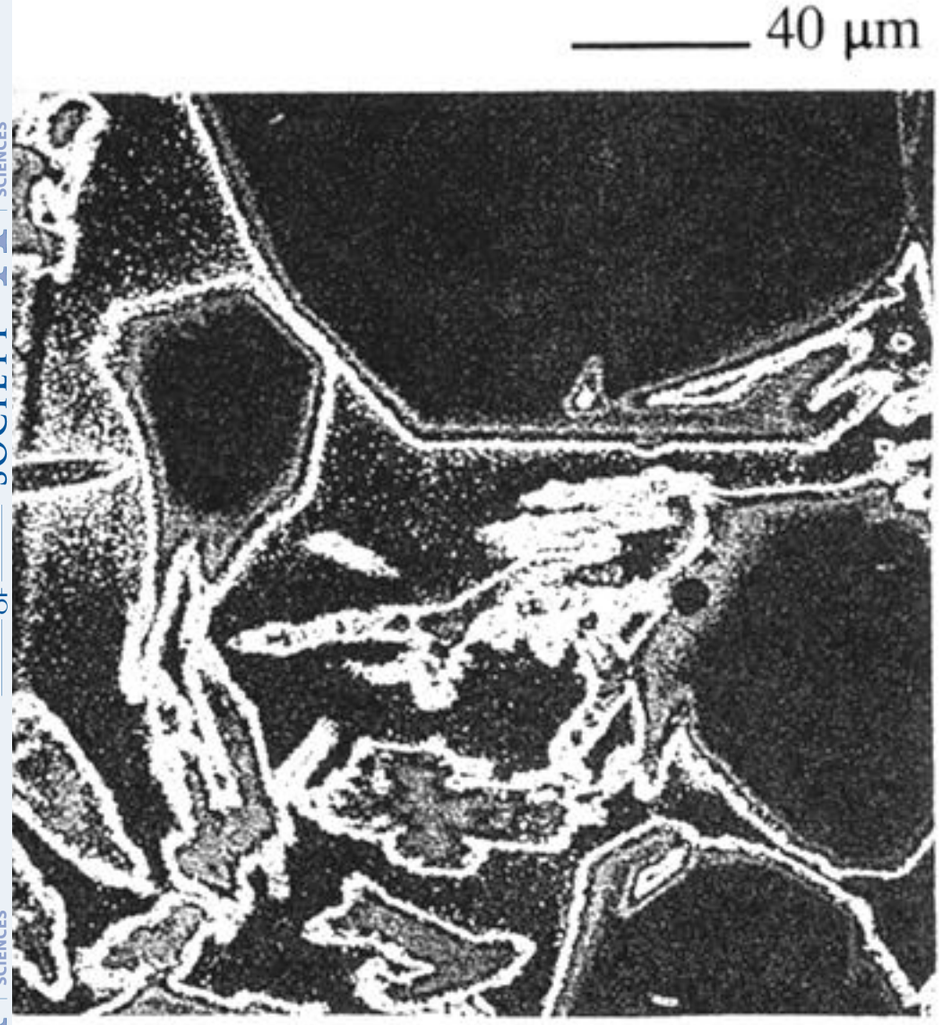

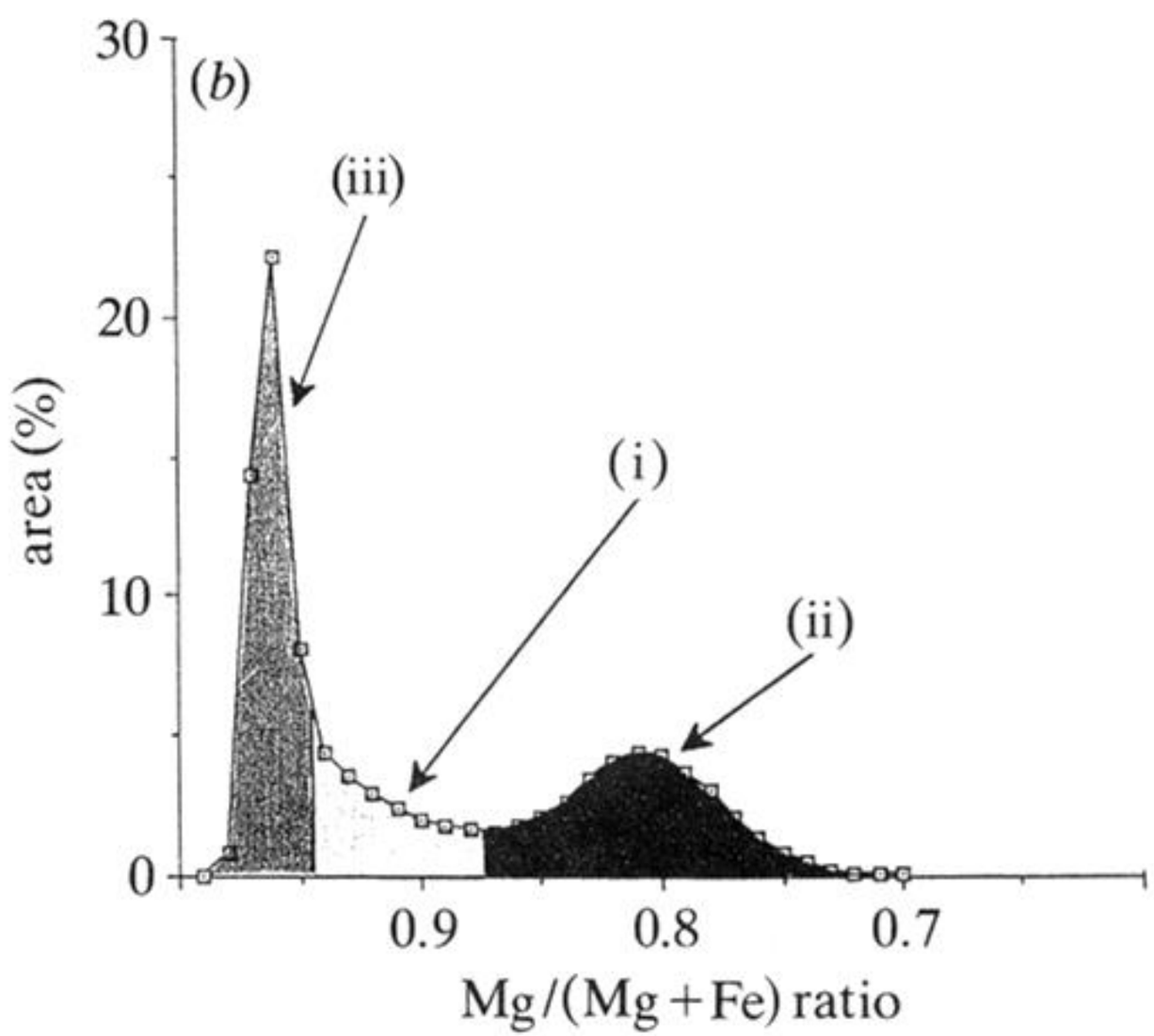

igure 6. Example of X-ray mapping analysis on experimental run product (1.5 GPa, 1650 °C, 0.5 h). (*a*) Concentration map of Mg, consisting of large euhedral olivines (50–200 μm), small yroxene quench crystals (10–50 μm) and glass. Olivines are mantled by thin rinds of overgrowth. riginal photo was in 24 pseudo colours corresponding to MgO concentration. Approximately 30 % the original area ($400 \times 400\ \mu m^{-2}$) is shown. (*b*) The Mg/(Mg + Fe) ratios of the 160000 point nalyses were computed by using a calibration line method. Quench crystals (i), overgrowth and ass (ii) can be distinguished from the stable olivine crystals (iii) by using the Mg/(Mg + Fe) ratios.